Pergamon

0038-1101(94)00197-9

Solid-State Electronics Vol. 38, No. 5, pp. 1009–1015, 1995

0038-1101/95 $9.50 + 0.00

ANALYSIS OF INTERNAL QUANTUM EFFICIENCY AND A NEW GRAPHICAL EVALUATION SCHEME

MICHÈLE HIRSCH, UWE RAU and JÜRGEN H. WERNER
Max-Planck-Institut für Festkörperforschung, Heisenbergstraße 1, D-70569 Stuttgart, Germany

(Received 17 May 1994; in revised form 23 August 1994)

Abstract—The analysis of internal quantum efficiency data is extended by a new graphical evaluation scheme. On the one hand, our method allows one to estimate the minority carrier diffusion length L and the back surface recombination velocity S. On the other hand the limitations of the internal quantum efficiency method are studied. A mathematical treatment of the equations describing internal quantum efficiency demonstrates that already a single measurement of either the effective diffusion length L_{eff} measured in the near infrared, or the collection efficiency η_c measured in the near bandgap wavelength range, yields *limits* for L and S. More precise values can be obtained in specific cases, if the analysis of L_{eff} and η_c are combined. In those cases, information about the accuracy of L and S is obtained. We present a graphical solution for the evaluation and illustrate our method using quantum efficiency data from both thick and thin silicon solar cells.

NOTATION

D	diffusion constant of the minority carriers in the base
e_{rel}	relative error of the measuring values
F_0	limit $\lim_{s\to 0} l_{\text{eff}}$
F_∞	limit $\lim_{s\to\infty} l_{\text{eff}}$
$\mathscr{F}_1$	limit $\lim_{s\to 0} \eta_c$
$\mathscr{F}_\infty$	limit $\lim_{s\to\infty} \eta_c$
G_∞	limit $\lim_{l\to\infty} l_{\text{eff}}$
$\mathscr{G}_\infty$	limit $\lim_{l\to\infty} \eta_c$
IQE_1	intercept of second linear regime ($L_\alpha \gg W$) in Fig. 1
L	bulk diffusion length of the minority carriers in the base
l	reduced bulk diffusion length
L_1	characteristic length in Fig. 1, in the case of $L_\alpha \gg W$
L_{eff}	effective diffusion length
l_{eff}	reduced effective diffusion length
$l_{\max}$	upper limit of the reduced bulk diffusion length
$l_{\min}$	lower limit of the reduced bulk diffusion length
L_α	absorption length of light
m_i, m_j, m	generalized measuring values (e.g. l_{eff} or η_c)
N_a	doping concentration of the base
N_{sub}	doping concentration of the substrate
p_k, p_l	generalized parameters (e.g. l and s)
S	back surface recombination velocity of the minority carriers in the base
s	reduced surface recombination velocity
$s_{\max}$	upper limit of the reduced surface recombination velocity
W	base width
α	absorption coefficient of light
Δ	cumulative error
η_c	collection efficiency
λ	wavelength of light

1. INTRODUCTION

The performance of a silicon solar cell is, to a large extent, determined by the recombination of minority carriers which are photo-generated in the base region of the cell. Therefore, knowledge is required concerning the parameters describing this recombination. The two most significant parameters are the recombination velocity S at the back surface and the bulk minority carrier diffusion length L in the base.

A measurement of the internal quantum efficiency (IQE) of the solar cell illuminated from the front side[1–3] as well as from the rear side in the case of bifacial solar cells[4] is well suited to this task. The IQE is defined as the number of collected minority carriers per incident photon of wavelength λ that is not reflected from the solar cell[1]. The IQE depends on the wavelength λ mainly through the absorption length $L_\alpha(\lambda) = \alpha^{-1}(\lambda)$, where $\alpha(\lambda)$ denotes the absorption constant. Basore[1,5] proposed the use of two different wavelength regimes for the quantitative evaluation of IQE data. Figure 1 illustrates a typical dependence of the inverse quantum efficiency IQE on the absorption length L_α for front side illumination; two wavelength regimes can be discerned as indicated by the two straight lines I and II.

The *conventional* analysis[5] of IQE data uses the wavelength range in the near infrared ($800 < \lambda < 1000$ nm for silicon cells), where the absorption length L_α is short when compared to the thickness W of the base of the solar cell ($L_\alpha \ll W$). Under these conditions a plot of $(\text{IQE})^{-1}$ vs L_α yields a straight line, illustrated by curve I in Fig. 1. The inverse slope of this line is the so-called effective diffusion length L_{eff}, which contains the bulk diffusion length L and the (back) surface recombination velocity S[5].

An *extended* analysis[1,5] of IQE-data uses, additionally, information from weakly absorbed,

larger wavelength light (λ in the near-bandgap regime) where $L_\alpha \gg W$ holds, (1080 nm $< \lambda <$ 1120 nm for silicon). In this regime, the wavelength dependence of the IQE suffers, apart from recombination losses, also from parasitic absorption and additional reflectance inside of the solar cells[1,2]. Nevertheless, again a linear dependence on L_α is observed as illustrated by curve II in Fig. 1. This regime yields an intercept $(\mathrm{IQE}_l)^{-1}$ and a characteristic length L_l from the inverse slope. The quantities IQE_l and L_l depend in a rather complicated way on the optical as well as on the electrical properties of the solar cell. However, it is possible to extract from L_l and IQE_l the so-called collection efficiency η_c that itself depends only on the electrical base properties, the two recombination parameters, S and L. A useful approximation is given by $\eta_c \approx \mathrm{IQE}_l$, where the accuracy of this approximation is influenced by the backside reflectance. Since in this wavelength regime also optical parameters influence the IQE measurement, we expect a higher uncertainty for η_c than for L_{eff}.

The separation of the two recombination parameters L and S is an important problem that must be solved because both L_{eff} and η_c depend on the implicit combination of L and S. In this paper, we discuss the information which can be obtained about the characteristic base parameters L and S, once the quantities L_{eff} and η_c are extracted from IQE measurements, e.g. as discussed in [1,2,5]. In Section 2, we concentrate on the effective diffusion length L_{eff}. Analyzing the equation for L_{eff}, we will demonstrate that even the knowledge of this *single* quantity restricts the allowed parameter range and leads to statements concerning (i) a minimum and maximum bulk diffusion length, or, (ii) a minimum bulk diffusion length and a maximum (back) surface recombination velocity. Furthermore, we give a simple criterion to decide from the value L_{eff}, which one of the two statements (i) or (ii) is valid. In a second step we present a general graphical evaluation scheme from which the values of the limits can directly be read. In Section 3, we demonstrate that the analogous statements (i) and (ii) can be developed for η_c. Section 4 discusses the combination of the two quantities L_{eff} and η_c. A sensitivity analysis shows that the accurate determination of both parameters L and S is restricted to a small part of the parameter plane put up by L and S themselves. In Section 5, we then apply the different evaluation schemes to some typical experimental data.

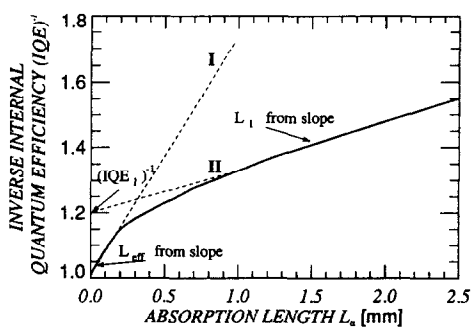

Fig. 1. The plot of inverse quantum efficiency vs absorption length L_α shows two linear regimes. The initial slope for small L_α (see I) yields the effective diffusion length L_{eff}. The asymptotic behavior in region II for large L_α yields an intercept $(\mathrm{IQE}_l)^{-1}$ and the characteristic length L_l from the inverse slope (see Ref. [1]).

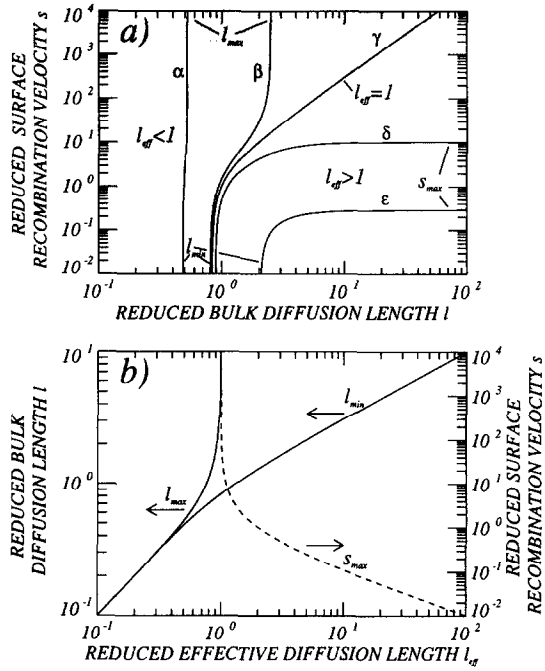

Fig. 2. (a) The parameter plane of l and s for l_{eff} is split into two parts. Values of $l_{\mathrm{eff}} < 1$ (gray part of the figure), contain information about a lower (l_{min}) and upper limit (l_{max}) for the bulk diffusion length l (see curve α for $l_{\mathrm{eff}} = 0.5$ and curve β for $l_{\mathrm{eff}} = 0.95$) for an either very large or very small surface recombination velocity s. Measured $l_{\mathrm{eff}} > 1$ (white part of the figure) give information on a lower limit l_{min} for l and an upper limit s_{max} for s (see curve δ for $l_{\mathrm{eff}} = 1.05$ and curve ϵ for $l_{\mathrm{eff}} = 4.5$). The boundary between the two regimes is defined by curve γ for $l_{\mathrm{eff}} = 1$ which only allows for the determination of a lower limit l_{min} of l. (b) For any measured l_{eff}, this figure allows for the direct graphical determination of lower and upper limit l_{min}, l_{max} for the bulk diffusion length l as well as for an upper limit s_{max} of the surface recombination velocity s.

2. THE EFFECTIVE DIFFUSION LENGTH L_{eff}

For the sake of generality we use the following dimensionless variables: the reduced diffusion length $l = L/W$, and the reduced surface recombination velocity $s = SW/D$. Here D denotes the minority carrier diffusivity. The reduced effective diffusion length $l_{\mathrm{eff}} = L_{\mathrm{eff}}/W$ is derived from IQE data from the relation $\mathrm{IQE}^{-1} = 1 + L_\alpha/(l_{\mathrm{eff}} W)$ and depends on the parameters l and s according to[1]:

$$l_{\mathrm{eff}}(l, s) = l\frac{sl\sinh(l^{-1}) + \cosh(l^{-1})}{sl\cosh(l^{-1}) + \sinh(l^{-1})}. \qquad (1)$$

With a measured value l_{eff} the feasible range for l and s is reduced to sets of points (l, s) which fulfill the condition $l_{\text{eff}}(l, s) = l_{\text{eff}}$. In Fig. 2(a), five exemplary curves for various values of l_{eff} are plotted in the parameter plane $\{l, s\}$. These curves represent the implicit functions $s(l)|_{l\text{eff}}$ or $l(s)|_{l\text{eff}}$.

The asymptotic behavior of the curves in Fig. 2(a) suggests a separation into two classes. (i) The first class of implicit functions $s(l)|_{l\text{eff}}$ is characterized by the occurrence of a finite, upper limit $l_{\max}$ for l when s becomes infinite and a second finite, lower limit $l_{\min}$ for l when s becomes zero. This case [see curves α, β in Fig. 2(a)] arises for $l_{\text{eff}} < 1$, which covers the gray part of the parameter plane $\{l, s\}$. (ii) The second class of implicit functions $l(s)|_{l\text{eff}}$, belong to the white part in Fig. 2(a). The curves asymptotically reach an upper limit $s_{\max}$ for the surface recombination velocity s when l becomes infinite (see curves δ, ϵ) and again a lower limit $l_{\min}$ for l when s becomes zero. The boundary between the two classes (or the two parts of the parameter plane) is given by the curve for $l_{\text{eff}} = 1$. Consequently, one can directly decide from the measured l_{eff} which of the two cases applies. It is then possible to give *either* upper and lower limits for l, *or* a lower limit for l and an upper limit for s. Mathematically exact, the above statements can be formulated as follows:

(i) If $l_{\text{eff}} < 1$ then $0 < s < \infty$ and $l_{\min} < l < l_{\max}$ hold.
From a measured $l_{\text{eff}} < 1$ an upper *and* a lower limit to l can be concluded.

(ii) If $l_{\text{eff}} > 1$ then $0 < s < s_{\max}$ and $l_{\min} < l < \infty$ hold.
An upper limit $s_{\max}$ for s and a lower limit $l_{\min}$ for l can be deduced if $l_{\text{eff}} > 1$ is measured.

(iii) If $l_{\text{eff}} = 1$ then $0 < s < \infty$ and $l_{\min} < l < \infty$ hold.
Only a lower limit $l_{\min}$ can be derived if $l_{\text{eff}} = 1$ is measured.

Next, we give relations that allow for the determination of the limits from the measured l_{eff}. Here one has to be aware that the limiting values $l_{\max}$ and $l_{\min}$ for the bulk diffusion length l cannot be found analytically because eqn (1) cannot be inverted in closed form with respect to l. The upper limit $s_{\max}$ for the surface recombination velocity s and the two limits $l_{\min}$ and $l_{\max}$ for the diffusion length l are derived from:

$$s_{\max} = G_\infty^{-1}(l_{\text{eff}}), \tag{2}$$

$$l_{\min} = F_0^{-1}(l_{\text{eff}}), \quad \text{and} \tag{3}$$

$$l_{\max} = F_\infty^{-1}(l_{\text{eff}}), \tag{4}$$

where G_∞^{-1}, F_0^{-1} and F_∞^{-1} are the inverse functions of:

$$G_\infty(s) = (s + 1)/s, \tag{5}$$

$$F_0(l) = l \coth(l^{-1}), \quad \text{and} \tag{6}$$

$$F_\infty(l) = l \tanh(l^{-1}). \tag{7}$$

The proof for the statements (i)–(iii) as formulated in the Appendix is essentially based on two properties of eqn (1): the monotony of the implicit functions and the existence of the four limits of l_{eff} for $l = 0$, $l = \infty$, $s = 0$ and $s = \infty$.

Figure 2(b) delineates the relations between the measured effective diffusion length l_{eff} and the three corresponding limits $l_{\min}$, $l_{\max}$ and $s_{\max}$. Here the relation $s_{\max} = (l_{\text{eff}} - 1)^{-1}$, which is the inverted eqn (5), is used explicitly, whereas eqns (6) and (7) are graphically inverted. Inserting any measured value l_{eff} on the abscissa, one finds the two limiting values appropriate for this special case for either $(l_{\min}, s_{\max})$ or $(l_{\min}, l_{\max})$ as the maximum information which can be extracted from the knowledge of only one single measured value. The use of dimensionless quantities, which requires the knowledge of only the base thickness, provides the possibility to use Fig. 2(b) as a simple and general evaluation scheme for experimental data. The knowledge of the diffusion constant D is, however, necessary to obtain the value of the back surface recombination velocity S from its reduced value s.

In contrast to our previous evaluation methods, which used a series expansion[6] *no a priori knowledge* or assumptions concerning the diffusion length l or surface recombination s is required here. However, from the analysis of Fig. 2(b), we find that the following approximations are valid in a specific range of l_{eff}. For $l_{\text{eff}} \geq 3$ it holds that $l_{\min} \approx \sqrt{l_{\text{eff}}}$ within an error of better than 6%, and for $l_{\text{eff}} \leq 0.4$ the approximation $l_{\min} \approx l_{\max} \approx l_{\text{eff}}$ holds to within 1%.

3. THE COLLECTION EFFICIENCY η_c

In addition to the reduced effective diffusion length l_{eff}, the extended IQE analysis also yields the collection efficiency[1]:

$$\eta_c(l, s) = l \frac{sl[\cosh(l^{-1}) - 1] + \sinh(l^{-1})}{sl \sinh(l^{-1}) + \cosh(l^{-1})}. \tag{8}$$

In Fig. 3(a) we show several implicit functions $s(l)|_{\eta_c}$ or $l(s)|_{\eta_c}$ for different values of η_c. Qualitatively these functions show the same characteristics with respect to their asymptotic behavior as those of l_{eff} in Fig. 2(a). The following three relations are found in complete analogy to Section 2:

(i) If $\eta_c < 0.5$ then $0 < s < \infty$ and $l_{\min} < l < l_{\max}$.
With a measured value $\eta_c < 0.5$ one finds an upper *and* a lower limit for l.

(ii) If $\eta_c > 0.5$ then $0 < s < s_{\max}$ and $l_{\min} < l < \infty$.
From a measured value $\eta_c > 0.5$ an upper limit $s_{\max}$ for s and a lower limit $l_{\min}$ for l can be deduced.

(iii) If $\eta_c = 0.5$ then $0 < s < \infty$ and $l_{\min} < l < \infty$.
Only a lower limit $l_{\min}$ for l can be extracted if $\eta_c = 0.5$ is measured.

The maximum surface recombination velocity $s_{\max}$ and the minimum and maximum diffusion lengths $l_{\min}$ and $l_{\max}$ are obtained from:

$$s_{\max} = \mathcal{G}_\infty^{-1}(\eta_c), \tag{9}$$

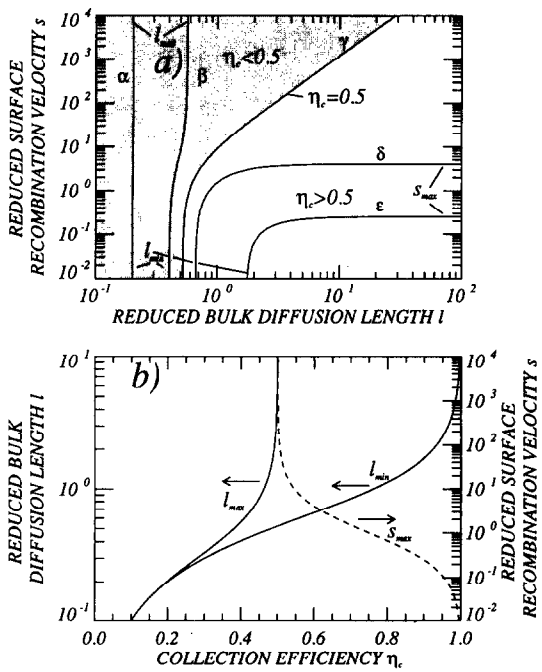

Fig. 3. (a) The parameter plane of l and s for η_c separates into two parts. Values of $\eta_c < 0.5$ (gray part of the figure), contain information about a lower (l_{min}) and upper limit (l_{max}) for the bulk diffusion length l (see curve α for $\eta_c = 0.2$ and curve β for $\eta_c = 0.4$) for an either very large or very small surface recombination velocity s. Measured $\eta_c > 0.5$ (white part of the figure) give information on a lower limit l_{min} for l and an upper limit s_{max} for s (see curve δ for $\eta_c = 0.6$ and curve ϵ for $\eta_c = 0.9$). The boundary between the two regimes is defined by curve γ for $\eta_c = 0.5$ which only allows for the determination of a lower limit l_{min} of l. (b) For any measured η_c, this figure allows for the direct graphical determination of lower and upper limit l_{min}, l_{max} for the bulk diffusion length l as well as for an upper limit s_{max} of the surface recombination velocity s.

$$l_{min} = \mathcal{F}_0^{-1}(\eta_c) \quad \text{and} \tag{10}$$

$$l_{max} = \mathcal{F}_\infty^{-1}(\eta_c), \tag{11}$$

where $\mathcal{G}_\infty^{-1}$, $\mathcal{F}_0^{-1}$ and $\mathcal{F}_\infty^{-1}$ are the inverse functions of:

$$\mathcal{G}_\infty(s) = \frac{s/2 + 1}{s + 1}, \tag{12}$$

$$\mathcal{F}_0(l) = l \tanh(l^{-1}) \quad \text{and} \tag{13}$$

$$\mathcal{F}_\infty(l) = l \frac{\cosh(l^{-1}) - 1}{\sinh(l^{-1})}. \tag{14}$$

The proof for relations (i)–(iii) is analogous to that discussed in the Appendix for l_{eff}.

Figure 3(b) presents the graphical evaluation for the information contained in the measurement of η_c. The value of $\eta_c = 0.5$ [see curve γ in Fig. 3(a)] separates the two parts of the parameter plane. Note that η_c is restricted to the range of $0 \leqslant \eta_c \leqslant 1$ and that η_c cannot be measured as accurately as l_{eff} because it is extracted from a wavelength regime where optical properties of the solar cell also influence the IQE measurement. With Fig. 3(b) and the knowledge of η_c one can find values l_{min}, l_{max} and s_{max}, which are in general different from those obtained from the measurement of l_{eff} for the same sample as can be seen by the comparison of Figs 2(b) and 3(b).

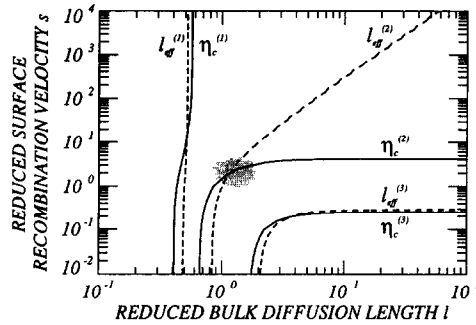

Fig. 4. Combination of the implicit functions l_{eff} and η_c in the parameter space $\{l, s\}$ (the three curves $l_{eff}^{(1)}$, $l_{eff}^{(2)}$, and $l_{eff}^{(3)}$ correspond to the values of $l_{eff} = 0.8$, 1.0 and 4.5, the three curves $\eta_c^{(1)}$, $\eta_c^{(2)}$, and $\eta_c^{(3)}$ correspond to the values of $\eta_c = 0.4$, 0.6 and 0.9). The shaded area has the highest sensitivity to l and s and it holds for the cumulative error $\Delta < 15\Delta e_{rel}$.

4. THE COMBINATION OF l_{eff} AND η_c

With the knowledge of both independently measured quantities l_{eff} and η_c, it should be possible, in principle, to deduce the two parameters of interest l and s exactly. However, it is not possible to solve eqns (1) and (8) with resect to l and therefore no closed expressions of l and s are available.

In the graphical delineation of the parameter plane $\{l, s\}$ the two unknown values (l, s) for a particular sample are indicated by the intersection of the curves belonging to the two independently measured quantities l_{eff} and η_c. This intersection shows different characteristics which are indicated by three representatives depicted in Fig. 4. The two curves $l_{eff}^{(1)}$, $\eta_c^{(1)}$ intersecting in the left part of the $\{l, s\}$-parameter plane both are nearly parallel to the s-axis and intersect each other under a very flat angle. Hence, an associated uncertainty of l and s will be predominantly in the s-direction. The two curves $l_{eff}^{(2)}$, $\eta_c^{(2)}$ intersecting in the middle of the graph intersect under a larger angle. This finding should allow for a better extraction of the corresponding intersection point. The two curves $l_{eff}^{(3)}$, $\eta_c^{(3)}$ intersecting in the lower right corner again are nearly parallel to each other and therefore intersect again under a smaller angle. Here the uncertainty is more likely to be associated with the l-direction.

A quantitative description of the uncertainty associated with a parameter pair (l, s) is facilitated by the following notation: the measuring values are identified with $l_{eff} = m_1$ and $\eta_c = m_2$ to use now m_i, m_j (with $i, j = 1, 2$), and the parameters $l = p_1$ and $s = p_2$ with p_l, p_k (with $k, l = 1, 2$). We use the cumulative error $\Delta^2 := \Sigma_{k=1,2} (\Delta p_k / p_k)^2$, i.e. the sum of the relative variances of the parameters, as a measure for their

uncertainty. The relative variance $(\Delta p_k/p_k)^2$ is given by:

$$\left(\frac{\Delta p_k}{p_k}\right)^2 = \sum_{i=1,2}\left(\frac{\partial p_k}{\partial m_i}\right)^2\Big|_{m_j \neq i}\left(\frac{m_i}{p_k}\right)^2\left(\frac{\Delta m_i}{m_i}\right)^2, \quad (15)$$

where the partial derivatives can be given analytically by the known derivatives $\partial m_i/\partial p_k$ of the measured values with respect to the parameters by:

$$\frac{\partial p_k}{\partial m_i}\Big|_{m_j \neq i} = (-1)^{i+k}\frac{\partial m_j}{\partial p_i}\Big|_{p_k \neq i}\left[\det\left(\frac{\partial m_i}{\partial p_k}\right)\right]^{-1}, \quad (16)$$

where the last term is the inverse of the Jacobian of the linearized equations. Assuming for simplicity the same relative errors $\Delta m_i/m_i = e_{rel}$ for both measuring values yields Δ as a linear function of e_{rel} for each pair (l, s). To compare the sensitivity of different combinations (l, s), it is sufficient to use the prefactor determined by the partial derivatives defined by eqn (16). In Fig. 4 the shaded area near the middle of the parameter plane belongs to the part where the cumulative error $\Delta < 15e_{rel}$. For example, a relative error for both measured values l_{eff} and η_c of 1% results in a cumulative error of l and s that is smaller than 15%. This sensitivity to both parameters applies with the dimensionless parameters l and s being approximately in the range $(0.8 < l < 1.9$ and $0.95 < s < 4.7)$. In the following we denote this area of small cumulative error as the *sensitivity area* of the IQE measurement (see Fig. 4).

We note that a similar discussion as above has *qualitatively* been led in Ref. [1] using the complementary parameter plane of the measuring values $\{l_{eff}, \eta_c\}$. The sensitivity area obtained from our quantitative treatment may be transformed from the $\{l, s\}$-plane into the $\{l_{eff}, \eta_c\}$-plane by eqns (1) and (8). It turns out that an evaluation of experimental data in terms of both parameters l and s only makes sense if the *measured values* l_{eff} and η_c fall in the sensitivity range $0.6 < l_{eff} < 1.5$ and $0.5 < \eta_c < 0.74$. Figure 5 displays a magnified view of the sensitivity area in the $\{l, s\}$-plane including a useful set of curves for constant l_{eff} (solid lines) and for constant η_c (dotted lines).

Figure 5 can be used as a graphical evaluation scheme in order to determine the bulk diffusion

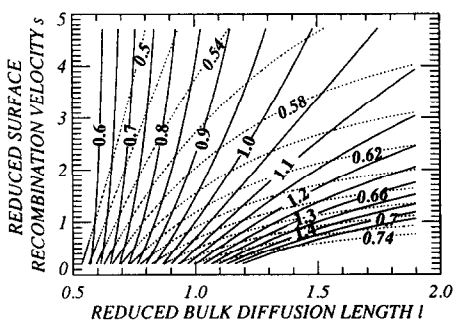

Fig. 5. Magnified plot of the area with the highest sensitivity to l and s. From l_{eff} (——) and η_c (· · · · ·) one choses the appropriate lines for the measurement. The coordinates of their intersection yield the diffusion length l and surface recombination velocity s.

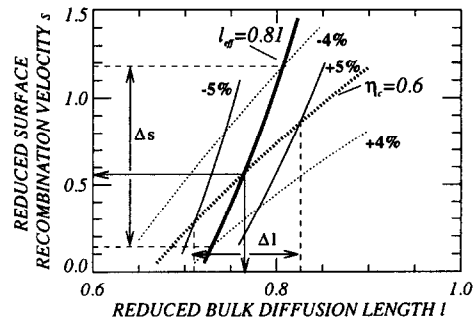

Fig. 6. Evaluation of a sample from Ref. [1]. From the intersection of the curves for the measured $l_{eff} = 0.81 \pm 5\%$ and $\eta_c = 0.6 \pm 4\%$ a value of $l = 0.76$ is deduced from the abscissa and $s = 0.57$ from the ordinate. The intersections of the lines of the corresponding uncertainty yield the uncertainty for l with $\Delta l = \pm 0.1$ and for the surface recombination velocity s with $\Delta s = 0.57^{+0.61}_{-0.43}$.

length l and the surface recombination velocity s. With a pair of measured values (l_{eff}, η_c) one looks for the two curves which belong to these two values. From the coordinates of the intersection point, the reduced values for the recombination velocity s and the diffusion length l are found. Additionally from Fig. 5 it is possible to access graphically the error for the measurement. The neighboring lines $(l_{eff} \pm \Delta l_{eff})$ and $(\eta_c \pm \Delta\eta_c)$ define a rhomb in the parameter-space $\{l, s\}$ which in turn yields the error bars for l and s as projections to the respective axes.

5. APPLICATION TO EXPERIMENTAL DATA

The application of our evaluation scheme to some typical experimental data is covered next. Basore discussed[1] solar cell structures of 10 Ωcm p-type silicon with a base width $W = 640\ \mu$m. His reported value of $L_{eff} = 260\ \mu m \pm 5\%$ corresponds to $l_{eff} = 0.41 \pm 5\%$, additionally the collection efficiency is reported as $\eta_c = 0.43 \pm 8\%$. These values do not belong to the area of small cumulative error, a statement concluded from Fig. 5: the curves corresponding to $l_{eff} = 0.41$ as well as to $\eta_c = 0.43$, lie outside of the sensitivity regime. We therefore apply the evaluation scheme for l_{eff} of Section 2. We find $l_{min} \approx l_{max} \approx l_{eff} = 0.41 \pm 5.4\%$ within the error of $\pm 5.4\%$. On the other hand, applying the evaluation scheme for η_c from Fig. 3(b) yields values of $l_{min} = 0.44 \pm 8\%$ and $l_{max} = 0.7 \pm 29\%$. These two values are consistent, within the given estimates. However, the analysis of l_{eff} yields obviously a smaller permitted range for l and therefore yields the better information.

Another solar cell presented in Ref. [1] consisted of 2 Ωcm p-type silicon with a base width $W = 470\ \mu$m. The measured values were reported as $L_{eff} = 380\ \mu m \pm 5\%$ (i.e. $l_{eff} = 0.81 \pm 5\%$) and $\eta_c = 0.6 \pm 4\%$. In this case, Fig. 5 can be used for the evaluation. In Fig. 6 we show only the relevant lines for this particular solar cell to demonstrate the appropriate values for l and s as well as their

corresponding error. We find for the values of the parameters $l = 0.76$ and $s = 0.57$. Our results for the surface recombination velocity $S = sD/W = 390\,\text{cm/s}$ (using a diffusion constant of $D = 32\,\text{cm}^2/\text{s}$) and the minority carrier diffusion length $L = lW = 360\,\mu\text{m}$ agree with the values given in Ref. [1] where the diffusion length was reported as $L = 350\,\mu\text{m}$ and the surface recombination velocity as $S = 400\,\text{cm/s}$. The error is found in Fig. 6 by inspecting the curves appropriate to the estimated error range ($\pm 5\%$ for L_{eff} and $\pm 4\%$ for η_c). This procedure yields the uncertainty of s resulting mainly from the uncertainty in η_c and the range of s includes $s = 0.14$ as the lowest and $s = 1.18$ as the highest value ($s = 0.57^{+0.61}_{-0.43}$). The uncertainty of l is mainly caused by the uncertainty of l_{eff} and the range of l includes $l = 0.71$ as the lowest and $l = 0.81$ as the highest value ($l = 0.76 \pm 0.5$). The measured values in this case lie outside the sensitivity area shown in Fig. 4.

As a third example, we use our own data reported in [6] for a thin film solar cell with a small base width. The cell consisted of p-type silicon, epitaxially grown by liquid phase epitaxy on a low resistivity Si-substrate, with a doping of $N_{\text{sub}} = 5 \times 10^{18}\,\text{cm}^{-3}$. The cell had a base of width $W = 16.8\,\mu\text{m}$ and a doping concentration $N_a = 1.5 \times 10^{17}\,\text{cm}^{-3}$. The diffusion length in the substrate is small and a contribution to the quantum efficiency of carriers collected from the substrate had not to be taken into consideration especially when using absorption lengths between 1 and $5\,\mu\text{m}$ for the determination of l_{eff}[6]. The reduced diffusion length was $l_{\text{eff}} = 12$ which clearly exceeds the value of one. Therefore, the application of the evaluation scheme of Fig. 2(b) yields information about $l_{\min}$ and $s_{\max}$. With this high value of l_{eff}, it is reasonable to use the relation $l_{\min} = \sqrt{l_{\text{eff}}} = 3.4 \pm 2.6\%$ and for the upper limit of the surface recombination velocity we find $S_{\max} = 800\,\text{cm/s} \pm 5.4\%$, using a diffusion constant $D = 15\,\text{cm}^2/\text{s}$[7] and an estimated error of 5% for L_{eff}.

These three experimental results are representative for all situations which may occur in experiment. The first and the third example cover the two cases where either minimum and maximum diffusion lengths can be extracted, or a minimum diffusion length and a maximum surface recombination velocity can be deduced. In both of these two cases these limiting values can be given with high precision, i.e. these limits do not depend sensitively on the accuracy of the measuring values l_{eff} or η_c. Furthermore, if one recombination path is obviously the dominant one these limits represent accurate values for this dominant parameter. The second example belongs to the case where the combination of l_{eff} and η_c allows us to deduce directly the values for l and s. Therefore, for this case a determination of both parameters l and s is possible, but one has to be aware of the errors which easily reach the order of several 10%.

6. CONCLUSIONS

A single measurement of either the effective diffusion length L_{eff} or the collection efficiency η_c yields information on limits of the bulk diffusion length L and the (back) surface recombination velocity S. We have here proposed a novel evaluation scheme [see Figs 2(b) and 3(b)] which allows one to deduce these limits directly from the measurements. All necessary information for evaluation can be extracted from the measurement itself and therefore no a priori knowledge is needed for this evaluation scheme.

We have also investigated the sensitivity of the combination of l_{eff} and η_c to deduce the parameters l and s. This sensitivity analysis yields a range in the parameter plane $\{l, s\}$ where the cumulative error is small. Therefore, in this range the sensitivity to both parameters is high (see Fig. 5). A second graphical evaluation method (see Fig. 6) applies in this region and yields l and s as well as their accuracy.

We emphasize that the ideas underlying our evaluation scheme can be generalized to other experimental methods for the determination of l and s. Implicitly using the same arguments as above, limits for l and s were given earlier for the evaluation of internal quantum efficiency of cells measured under rear side illumination[4]. For such cells, IQE data depend sensitively on the back surface recombination velocity. However, the evaluation method of Ref. [4] is not applicable to solar cells with a non-transparent back surface. Generally speaking, only the monotonic dependence of the measured quantity m (where m represents a general variable for any appropriate measured quantity) on the parameters l and s as well as the existence of the limits $\lim_{l,s\to 0} m$ and $\lim_{l,s\to\infty} m$ is required to develop analogous evaluation schemes.

Acknowledgments—The authors gratefully acknowledge the support of H. J. Queisser as well as discussions with S. Kolodinski, R. Brendel, J. White and M. Schöfthaler. We thank H. Fischer of the University of Tübingen for the fruitful discussions concerning the mathematical aspects. Part of this work is supported by the German *Bundesministerium für Forschung und Technologie* under contract No. 01 M2920 A.

REFERENCES

1. P. A. Basore, *Proc. 23rd IEEE Photovoltaic Specialists Conf.*, p. 147. IEEE Publishing Service, New York (1993).
2. S. Kolodinski, Ph.D. thesis, Stuttgart. Unpublished.
3. H. J. Hovel, *Semiconductors and Semimetals* (Edited by R. K. Willardson and A. C. Beer), Vol. 11, p. 24. Academic Press, New York (1975).
4. J. C. Jimeno, A. Cuevas and A. Luque, *Proc. 18th IEEE Photovoltaics Specialists Conf.*, p. 726. IEEE Publishing Service, New York (1985).
5. P. A. Basore, *IEEE Trans. Electron. Dev.* **ED-37**, 337 (1990).
6. J. H. Werner, S. Kolodinski, U. Rau, J. K. Arch and E. Bauser, *Appl. Phys. Lett.* **62**, 2998 (1993).

7. J. K. Arch, E. Bauser, S. Kolodinski and J. H. Werner, *Proc. 11th Europ. Community Photovoltaic Sol. Energy Conf.*, p. 1047. Harwood Academic Publishers, Brussels (1993).

APPENDIX

Starting with eqn (1), that describes the dependence of l_{eff} on l and s, we find that it holds:

$$\partial l_{\text{eff}}/\partial l > 0, \quad \partial l_{\text{eff}}/\partial s < 0. \tag{A1}$$

The implicit function theorem yields the slope of the implicitly given functions $s(l)|_{l_{\text{eff}}}$. Note that with eqn (A1) we get $\partial s/\partial l = (-1)(\partial l_{\text{eff}}/\partial l)/(\partial l_{\text{eff}}/\partial s) > 0$, therefore we have a strongly monotonic increasing behavior of the implicit functions $s(l)$ and $l(s)$. In the next step we use the existence of the following limits:

$$\lim_{l \to 0} l_{\text{eff}} = 0 \tag{A2}$$

$$\lim_{l \to \infty} l_{\text{eff}} = (s+1)/s =: G_{\infty}(s) \in]1, \infty[\tag{A3}$$

$$\lim_{s \to 0} l_{\text{eff}} = l \coth(l^{-1}) =: F_0(l) \in]0, 1[\tag{A4}$$

$$\lim_{s \to \infty} l_{\text{eff}} = l \tanh(l^{-1}) =: F_{\infty}(l) \in]0, \infty[. \tag{A5}$$

In conjunction with the monotony of the functions $l_{\text{eff}}(l)$ for fixed s, and $l_{\text{eff}}(s)$ for fixed l [see eqn (A1)], we get the inequalities:

$$0 \leqslant l_{\text{eff}} \leqslant (s+1)/s, \tag{A6}$$

for fixed s and any value of l, and

$$l \tanh(l^{-1}) \leqslant l_{\text{eff}} \leqslant l \coth(l^{-1}), \tag{A7}$$

for fixed l and any value of s.

The boundaries or limits for the bulk diffusion length l and the surface recombination velocity s for a certain value of l_{eff} can be derived with the inequalities from eqns (A6), (A7): We need the strong monotony of $F_0(l)$, $F_{\infty}(l)$ and $G_{\infty}(s)$ in eqns (A3)–(A5) for the existence of their inverse functions $[F_0(l)]^{-1}$, $[F_{\infty}(l)]^{-1}$ and $[G_{\infty}(s)]^{-1}$. The sign of the monotony determines if the limits of the parameters l and s describe upper or lower bounds. Furthermore, it is necessary to take into account the range of the corresponding functions (A3)–(A5). These ranges yield the distinction of the three cases (i)–(iii) in Section 2 with $l_{\text{eff}} < 1$, $l_{\text{eff}} > 1$ and $l_{\text{eff}} = 1$ and finally the relations given in eqns (2)–(4).

We note that the result obtained from this Appendix appear visually obvious from Fig. 2 and this mathematical treatment may not be explicitly necessary for a two-dimensional parameter plane. However, the mathematical rigor demonstrated in this Appendix exemplarily for l_{eff} is, however, absolutely necessary in more general situations, where either the parameter plane is higher-dimensional or can not be so consequently normalized as in the present example.